

A MESHFREE METHOD FOR THE BGK MODEL FOR RAREFIED GAS DYNAMICS

S. TIWARI ^{*}, A. KLAR ^{*†} AND G. RUSSO [‡]

Abstract. In this paper we have applied a Semi-Lagrangian schemes with meshfree interpolation, based on a Moving Least Squares (MLS) method, to solve the BGK model for rarefied gas dynamics. Sod's shock tube problems are presented for a large range of Knudsen numbers in one dimensional physical space and three dimensional velocity space. In order to validate the solutions obtained from the meshfree method, we have used the piecewise linear Hermite interpolation. Furthermore, we have compared the solutions of the BGK model with the solutions obtained from Direct Simulation Monte Carlo (DSMC) method. In the case of a very small Knudsen number the numerical solutions are compared with the exact solutions of the compressible Euler equations. Overall we found that the meshfree interpolation gives better approximation than the Hermite interpolation.

Keywords. rarefied gas, kinetic equation, BGK model, meshfree method, semi-implicit method

1. Introduction. The Boltzmann equation is an evolution equation of a probability distribution function consisting of transport and collision terms [4]. Due to the high dimensional integral in the collision term, deterministic numerical approaches are complicated and time consuming. Therefore, stochastic numerical methods like DSMC, see [2, 1, 13], have been used extensively for complex applications. DSMC methods are suitable for high Mach number and stationary flows. However, for low Mach number flows, the statistical noise inherent in these methods dominates the flow quantities. Here, our main interest is to develop a numerical method for such low Mach number, time dependent flows in arbitrary geometries. Since last 20 years micro-nano scale rarefied gas flows have attracted many researchers due to the fabricated techniques in Micro-Electro-Mechanical-Systems (MEMS), [9], devices, for examples, micro pump, micro turbines, micro pipes [11]. We consider a simplified model for rarefied gas flows, where deterministic methods can be applied more easily. We choose a simplified model suggested by Bhatnager, Gross and Krook [10], the so called BGK model for the Boltzmann equation, where the collision term is replaced by a relaxation of the distribution function towards a local thermal equilibrium. For deterministic schemes for this model we refer to [12] and other references therein. In the present paper, we apply the Semi-Lagrangian scheme suggested by Russo and Filbet, see [14] for details. In contrast to [14], where one dimensional physical and one dimensional velocity spaces are considered, we consider here a three dimensional velocity space. Moreover, the reconstruction procedure is different compared to the one applied in [14]. Here, we use a meshfree method for the reconstruction. Meshfree methods are suitable for changing computational domains in time or flows in complicated geometries, see [16, 17]. we note that a meshfree method based on Least-squares was applied to solve the compressible Euler equations, see [8] and other references there.

The paper is organized as follows. In section 2 the BGK model for the Boltzmann equation is presented. In section 3 the semi Lagrangian scheme for the model and the boundary conditions are described. In section 4 we present piecewise linear Hermite interpolation and the moving least squares (MLS) approximation for the

^{*}Technische Universität Kaiserslautern, Department of Mathematics, Erwin-Schrödinger-Straße, 67663 Kaiserslautern, Germany ({klar, tiwari}@mathematik.uni-kl.de)

[†]Fraunhofer ITWM, Fraunhoferplatz 1, 67663 Kaiserslautern, Germany

[‡]Department of Mathematics and Computer Science, University of Catania, Italy (russo@dmi.unict.it)

reconstruction of the function. In section 5 Sod's shock tube problem [15] is solved for several range of Knudsen numbers. For larger Knudsen numbers the numerical solutions for the BGK model obtained from the piecewise linear Hermite and MLS interpolations are compared with the solutions obtained from the DSMC simulations of the Boltzmann equation. For a very small Knudsen number, we have compared the numerical solutions of the BGK model with the exact solutions of the compressible Euler equations. We found that the solutions obtained from the MLS approximation are closer to the DSMC results or the exact solutions than the solutions obtained from the Hermite interpolation. Moreover, we have compared numerical approaches based on continuous and discrete Maxwellians as suggested in [12]. We found that the use of discrete Maxwellian allows us to reduce the number of velocity grids, which is very important in higher dimensional cases from the memory as well as computational point of view. Finally, in section 6 some conclusions and future works are presented.

2. The BGK model for rarefied gas dynamics . The BGK model is the simplified model of the Boltzmann equation for a rarefied gas dynamics, where the collision term is modeled by a relaxation of the distribution function $f(t, x, v)$ to the Maxwellian equilibrium distribution. The is the evolution equation of the distribution function $f(t, x, v)$ and is given by the following initial boundary value problem

$$\frac{\partial f}{\partial t} + v_x \frac{\partial f}{\partial x} = \frac{1}{\tau}(M - f) \quad (2.1)$$

with $f(0, x, v) = f_0(x, v)$, $t \geq 0, x \in [a, b] \subset R, v \in R^3$ and some boundary conditions at a and b , which will be described in the next section. We denote $v = (v_x, v_y, v_z)$. Here τ is the relaxation time and M is the local Maxwellian given by

$$M = \frac{\rho}{(2\pi RT)^{3/2}} \exp^{-\left(\frac{|v-U|^2}{2RT}\right)}, \quad (2.2)$$

where the parameters ρ, U, T are macroscopic quantities, namely, density, mean velocity and temperature, respectively. Here, R is the universal gas constant. The macroscopic quantities ρ, U, T are computed from $f(t, x, v)$ as its moments. In this case we have denoted $U = (U_x, U_y, U_z)$. Let $\phi(v) = \left(1, v, \frac{|v|^2}{2}\right)$ be the collision invariants. The moments are defined by

$$(\rho, \rho U, E) = \int_{R^3} \phi(v) f(t, x, v) dv. \quad (2.3)$$

Here, E is the total energy density and it is related to the temperature through the internal energy

$$e(t, x) = \frac{3}{2}RT, \quad \rho e = E - \frac{1}{2}\rho|U|^2. \quad (2.4)$$

The relaxation time τ and the mean free path λ are related according to [5]

$$\tau = \frac{4\lambda}{\pi\bar{C}}, \quad (2.5)$$

where $\bar{C} = \sqrt{\frac{8RT}{\pi}}$ and the mean free path is given by

$$\lambda = \frac{k_b}{\sqrt{2\pi\rho R}d^2},$$

where k_b is the universal gas constant and d is the diameter of the gas.

3. Semi-Lagrangian scheme for the BGK model. To solve the BGK model, we have used the semi Lagrangian method suggested by Russo & Filbet, see [14] for details. This is an implicit method. In this paper we give a short description of the method. We consider constant time step Δt , uniform meshes in velocity space with mesh size Δv and in physical space not necessarily uniform meshes with average spacing Δx . Let t_{final} be the final time step of computation. The time steps are given by $t_n = n\Delta t, n = 0, 1, \dots$. The space discretization is obtained by generating grid points (regular or irregular) $x_i \in [a, b], i = 1, \dots, N_x$, where N_x is the total number of grid points in physical space. We note that the N_x grid points include interior as well boundary points $x_1 = a$ and $x_{N_x} = b$. Consider the N_v velocity grid points in each directions, where the uniform velocity grid size is given by $\Delta v = \frac{v_{max} - v_{min}}{N_v} = \frac{2v_{max}}{N_v}$. The x-component of velocity grids are defined by $v_j = v_{min} + (j-1)\Delta v, j = 1, \dots, N_v + 1$. Similarly, the y- and z- components are defined by v_k and v_l for $k, l = 1, \dots, N_v + 1$. Assuming that $f \rightarrow 0$ for $|v| > v_{max}$.

Let $f_{jkl} = f_{jkl}(t, x) = f(t, x, v_j, v_k, v_l)$. The evolution equation of $f_{jkl}(t, x)$ along the characteristics between time steps n and $n + 1$ is calculated from the Lagrangian form of the discrete BGK model

$$\frac{df_{jkl}}{dt} = \frac{1}{\tau}(M_{jkl} - f_{jkl}) \quad (3.1)$$

$$\frac{dx}{dt} = v_j \quad (3.2)$$

with initial conditions

$$x(t_n) = \tilde{x}, f_{jkl}(t_n) = f_{jkl}^n(\tilde{x}) = \tilde{f}_{jkl}^n, t \in [t_n, t_{n+1}] \quad (3.3)$$

together with boundary conditions for f_{jkl} at boundary points.

Here M_{jkl} is still the local Maxwellian having the same moments of f_{jkl} and is re-expressed by

$$M_{jkl} = \frac{\rho}{(2\pi RT)^{3/2}} \exp\left(-\frac{(v_j - U_x)^2 + (v_k - U_y)^2 + (v_l - U_z)^2}{2RT}\right). \quad (3.4)$$

We solve Eq. (3.1) by the implicit Euler scheme

$$f_{ijkl}^{n+1} = \tilde{f}_{ijkl}^n + \frac{\Delta t}{\tau}(M_{ijkl}^{n+1} - f_{ijkl}^{n+1}), \quad (3.5)$$

and the characteristic equation (3.2) is solved by

$$x_i^{n+1} = \tilde{x}_{ijkl} + v_j \Delta t, \text{ for } i = 1, \dots, N_x, j, k, l = 1, \dots, N_v + 1, \quad (3.6)$$

where the initial position \tilde{x}_{ijkl} has to be determined. In Figure 3.1 we have given the geometrical interpretation. At the time level t^n all values $f_{ijkl}^n, i = 1, \dots, N_x$ are known. At the time level t^{n+1} the corresponding values are $f_{ijkl}^{n+1}, i = 1, \dots, N_x$.

The method consists of three steps:

(i) First, we determine \tilde{x}_{ijkl} from the backward characteristics $\tilde{x}_{ijkl} = x_i^{n+1} - v_j \Delta t$, see figure 3.1. Then, we reconstruct (or interpolate) the function \tilde{f}_{ijkl}^n at \tilde{x}_{ijkl} from the values of its neighboring grid points. One can use any reconstruction, for example piecewise Hermite interpolation, least squares interpolations. In this paper we use the piecewise Hermite linear interpolation and the linear least squares interpolation.

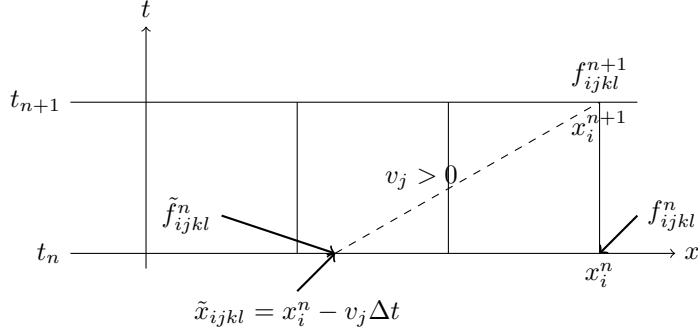


Fig. 3.1: Computational grid points in space and time

Higher order interpolations are also possible, for examples, piecewise cubic Hermite polynomial [14], WENO reconstruction [3].

(ii) In the second step we obtain M_{ij}^{n+1} . Since M_i^{n+1} and f_i^{n+1} give same conservative moments, we multiply above discrete equation (3.5) by collisional invariants $\phi(v)$ and sum over the velocity, we get

$$\rho_i^{n+1} = \sum_{j=1}^{N_v+1} \sum_{k=1}^{N_v+1} \sum_{l=1}^{N_v+1} \tilde{f}_{ijkl}^n \Delta v^3 \quad (3.7)$$

$$(\rho U_x)^{n+1} = \sum_{j=1}^{N_v+1} \sum_{k=1}^{N_v+1} \sum_{l=1}^{N_v+1} v_j \tilde{f}_{ijkl}^n \Delta v^3 \quad (3.8)$$

$$(\rho U_y)^{n+1} = \sum_{j=1}^{N_v+1} \sum_{k=1}^{N_v+1} \sum_{l=1}^{N_v+1} v_k \tilde{f}_{ijkl}^n \Delta v^3 \quad (3.9)$$

$$(\rho U_z)^{n+1} = \sum_{j=1}^{N_v+1} \sum_{k=1}^{N_v+1} \sum_{l=1}^{N_v+1} v_l \tilde{f}_{ijkl}^n \Delta v^3 \quad (3.10)$$

$$E_i^{n+1} = \frac{1}{2} \sum_{j=1}^{N_v+1} \sum_{k=1}^{N_v+1} \sum_{l=1}^{N_v+1} (v_j^2 + v_k^2 + v_l^2) \tilde{f}_{ijkl}^n \Delta v^3. \quad (3.11)$$

Now from (3.7 - 3.11) together with (2.4) we obtain all five parameters of Maxwellian and can define M_{ijkl}^{n+1} from (3.4).

(iii) Finally, we update the density function by

$$f_{ijkl}^{n+1} = \frac{\tau \tilde{f}_{ijkl}^n + \Delta t M_{ijkl}^{n+1}}{\tau + \Delta t} \quad \text{for } i = 1, \dots, N_x, \quad j, k, l = 1, \dots, N_v + 1. \quad (3.12)$$

3.1. Boundary conditions. We use the diffuse reflection boundary conditions. This means, when gas molecules hit boundaries, we forget their history. We reflect them according to the half Maxwellian with the wall density ρ_w , wall temperature T_w and wall velocity U_w . Let n be the unit normal on the wall pointing towards to the computational domain. In the case of Hermite interpolation we need ghost points next to the boundary points i in order to compute \tilde{f}_{ijkl}^n . The values of distribution

function are extrapolated from the interior grid points and then correct the distribution function according to the boundary condition. But in the case of the MLS interpolation, we first compute f_{ijkl}^{n+1} in all interior points i , then we extrapolate the new distribution function f_{Γ}^{n+1} for $(v - U_w) \cdot n > 0$ on the boundary points. For $(v - U_w) \cdot n < 0$ the diffuse reflection boundary conditions are obtained according to

$$M_{\Gamma}^{n+1} = \frac{\rho_w}{(2\pi RT_w)^{3/2}} \exp^{-\frac{|v-U_w|^2}{2RT_w}}, \quad (3.13)$$

where

$$\rho_w = -\frac{\int_{(v-U_w) \cdot n < 0} (v - U_w) \cdot n f_{\Gamma}^{n+1} dv}{\int_{(v-U_w) \cdot n > 0} (v - U_w) \cdot n \frac{1}{(2\pi RT_w)^{3/2}} \exp^{-\frac{|v-U_w|^2}{2RT_w}} dv}.$$

4. Interpolation methods. As we have already mentioned that our main aim is to develop a method to simulate the interactions of rigid body motion and rarefied gas. Due to the movement of a rigid body the computational domain for a gas changes, therefore, this is a time dependent problem. Moreover, the intersection of the surface of a rigid body and cells of rarefied gas makes numerical scheme more complicated. In the vicinity of a moving rigid body the regular grid structure does not exist any more. In this section we present two interpolation methods, which are suitable for irregular grids. In this paper we consider linear interpolation. Higher order interpolations require some stable reconstructions, like WENO, which will be focused in future works.

4.1. Piecewise linear Hermite interpolation. This is simple to implement and faster than the MLS method. However, one has to add the ghost points to apply boundary conditions, which could be complicated for complex boundaries. Let $I_k = [x_k, x_{k+1}] \subset [a, b]$ be an arbitrary interval and $x \in [x_k, x_{k+1}]$ be an arbitrary point. The corresponding function values are $f_k = f(x_k)$ and $f_{k+1} = f(x_{k+1})$. The linear interpolation at x is given by

$$f(x) = f_k + \frac{f_{k+1} - f_k}{x_{k+1} - x_k} (x - x_k) = \frac{f_k(x_{k+1} - x) + f_{k+1}(x - x_k)}{x_{k+1} - x_k}. \quad (4.1)$$

We note that the size of intervals I_k need not to be equal.

4.2. Moving least squares (MLS) interpolation. In contrast to Hermite interpolation, this is a fully meshfree method. In the Hermite interpolation, only the next left and right grid points are used to interpolate. However, in the MLS approximation, we use the nearest neighbor points inside a radius, which is about 3 times the average grid space. Therefore, the computational costs increase slightly in the case of MLS approximation compared to Hermite interpolation. But the MLS gives better approximation than the Hermite interpolation. In this case also the distribution of grids need not to be uniform. Another advantage of this method is that it is not required to add the ghost points to apply the boundary conditions and is easy to handle complex geometries.

Let $x \in [a, b]$ be an arbitrary point. We consider the problem to approximate the function $f = f(x)$ at x from the values of its neighboring points. We associate a weight function such that the near particles have higher and far particles have lesser influence. In order to limit the number of points the neighboring points are taken those points inside the circle of radius h with center x . We choose the radius

h , for example, some factor of Δx , such that we have at least minimum number of neighbors for the least squares approximation. Let $P(x) = \{x_j, j = 1, \dots, m\}$ be the set of m neighbor points of x inside the radius h . For the consistency the neighboring particles should not be on the same point. We note that this neighboring list is similar to the central stencils in the sense of the finite difference method. Therefore, if the relaxation time τ is very small and the solution of the Boltzmann equation develop shocks, we need to sort out the neighbor list according to the sign of the velocity v_x . For example, if $v_x > 0$ we select the neighbor of x $\{x_j \leq x, j = 1, \dots, m\}$ inside the radius h . Similarly, for negative velocity, we select the neighbor lists from the right side. The weight function can be quite arbitrary, but in our computations, we consider a Gaussian weight function

$$w(x_i - x; h) = \begin{cases} \exp(-\alpha \frac{(x_i - x)^2}{h^2}), & \text{if } \frac{|x_i - x|}{h} \leq 1 \\ 0, & \text{else,} \end{cases}$$

with α a user defined positive constant. In our computation, we have considered $\alpha = 6$. Let us sort out the neighboring points from 1 to m with respect to distance. This means, the neighbor index 1 is the nearest neighbor of x .

In order to approximate the function we consider the m Taylor's expansions of $f(x_j)$ around x

$$f(x_j) = f(x) + (x_j - x) \frac{\partial f}{\partial x} + e_j, \quad (4.2)$$

for $j = 1, \dots, m$, where e_j is the error in the Taylor's expansion. We first assume that f approximates the nearest point f_1 . In other words, $e_1 = 0$. The unknowns $f, \frac{\partial f}{\partial x}$ are computed by minimizing the error e_i for $i = 2, \dots, m$ and setting the constraint $e_1 = 0$. To solve this constraint least squares problem, we subtract the first equation with $e_1 = 0$ to all the other equations and the system of equations can be rewritten in the form

$$\begin{aligned} f_2 - f_1 &= (x_2 - x_1) \frac{\partial f}{\partial x} + e_2 \\ &\vdots \\ f_m - f_1 &= (x_m - x_1) \frac{\partial f}{\partial x} + e_m \end{aligned} \quad (4.3)$$

The system of equations can be written in the vector form as

$$e = b - M \frac{\partial f}{\partial x}, \quad (4.4)$$

where $e = [e_2, \dots, e_m]^T$, $b = [f_2 - f_1, \dots, f_m - f_1]^T$ and $M = [x_2 - x_1, \dots, x_m - x_1]^T$. For $m > 2$, this system of equations is over-determined for one unknown $[\frac{\partial f}{\partial x}]$. The unknown $\frac{\partial f}{\partial x}$ is obtained from the weighted least squares method by minimizing the quadratic form

$$J = \sum_{j=2}^m w_j e_j^2 = (M \frac{\partial f}{\partial x} - b)^T W (M \frac{\partial f}{\partial x} - b), \quad (4.5)$$

where $W = w_j \delta_{jk}, k = 2, \dots, m$ is the diagonal matrix. The minimization of J formally yields

$$\frac{\partial f}{\partial x} = (M^T W M)^{-1} (M^T W) b = \frac{\sum_{j=2}^m w_j (x_j - x_1) (f_j - f_1)}{\sum_{j=2}^m w_j (x_j - x_1)^2}. \quad (4.6)$$

Now from the equation (4.2) with $e_1 = 0$ for the closest point x_1 we can compute the value of $f(x)$ as

$$f(x) = f(x_1) + (x - x_1) \frac{\partial f}{\partial x} \quad (4.7)$$

since $\frac{\partial f}{\partial x}$ is now known. We note that the higher order approximations are straightforward. Moreover, the approximation in two and three dimensional physical space is also straight forward. We refer to our earlier papers [16, 17].

5. Numerical results. We have considered the Sod's shock tube problem [15] as Benchmark to validate our numerical methods. We consider the computational domain $[a, b] = [0, 1]$. The initial conditions are

$$\rho^0 = \rho_l, \quad U^0 = 0, \quad e^0 = 2.5 \quad \text{for } 0 \leq x < 0.5$$

$$\rho^0 = \rho_r, \quad U^0 = 0, \quad e^0 = 2.0 \quad \text{for } 0.5 \leq x \leq 1$$

with $\rho_l = 8 \times \rho_r$. We consider the following boundary conditions

$$U(t) = 0, \quad e(t) = 2.5 \quad \text{at } x = 0 \quad \text{and} \quad U(t) = 0, \quad e(t) = 2 \quad \text{at } x = 1.$$

In the MLS we set $\alpha = 6.0$ in (4.2) and h equal to 2.5 times the initial spacing of the grids. The initial spacing of the grids is given by $dx = 1/N_x$. We consider the monoatomic gas with diameter $d = 0.368 \times 10^{-9}m$, Boltzmann constant $k_b = 1.3806 \times 10^{-23}J K^{-1}$ and the universal gas constant $R = 208J kg K^{-1}$. The corresponding initial temperature are $0.008012 K$ on the left half of the domain and $0.00641 K$ on the right half of domain. The limit of the velocities in all direction is set by $v_{min} = -10m/s, v_{max} = 10m/s$. So, initially the gas is distributed according to the Maxwellian with these initial parameters. The final time is $t_{final} = 0.17$ seconds. The time step is $\Delta t = 0.00025$ second.

5.1. Test 1: Comparison of solutions in regular vs irregular grids. As a first test case we present the comparison of the numerical solutions in regular as well as irregular grids. We have considered $N_x = 200$. The regular grids are generated according to $x_i = i * \Delta x, i = 1, \dots, N_x$. To create the irregular grids we have moved the regular grids with velocity ± 1 times the random number and with time step $\Delta x/20$ for $i = 2, \dots, N_x - 1$. This movement is performed for 10 iterations. The density are $\rho_l = 5 \times 10^{-6}kg m^{-3}$ and $\rho_r = 0.125 \times 10^{-6}kg m^{-3}$. The corresponding Knudsen numbers are 0.02 on the left and 0.17 on the right half of the domain, where the characteristic length is $L = 1$. The corresponding relaxation times are 0.01 on the left half of the domain and 0.0957 on the right half of the domain. The flow is in transition regime. The initial condition is the Maxwellian distribution (2.2) with parameters given by the initial density, mean velocity and the temperature. In Figure 5.1 we have plotted the densities obtained from the MLS and the Hermite interpolations in regular as well as irregular grids. We observe that the irregular grids make no difference to the solutions obtained from the regular grids.

5.2. Test 2. In this case, we have compared the numerical solutions obtained from the BGK model with the DSMC simulations [1, 13] for the Boltzmann equation since DSMC results are widely used as Benchmark solutions. All parameters are same as in the Test 1. For DSMC simulations we have considered 200 cells and 400 gas

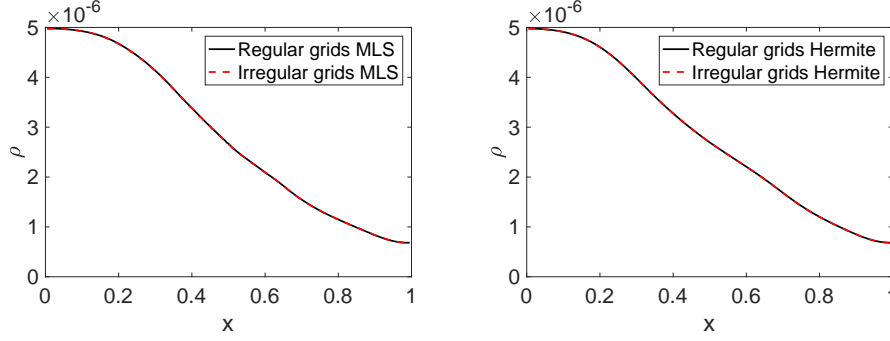


Fig. 5.1: Comparison of density for regular vs irregular grids. Left: MLS interpolation and Right: Hermite interpolation.

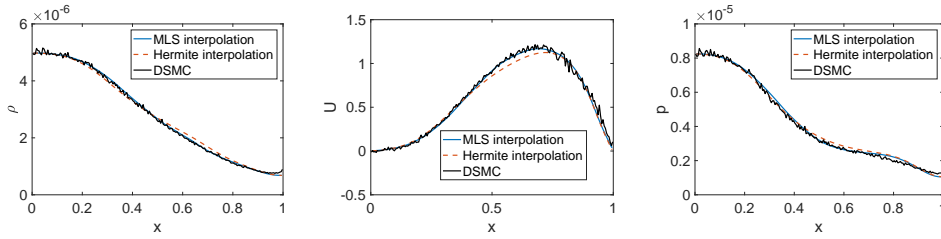


Fig. 5.2: Comparison of density, velocity and pressure obtained from MLS reconstruction, Hermite interpolation and DSMC for Knudsen number $Kn = 0.02$ on the left and $Kn = 0.17$ on the right.

molecules are initially generated per cell according to the Maxwellian distribution in the velocity, where the initial density, temperature and velocity are its parameters. The time steps of *DSMC* are same as in the semi Lagrangian scheme for the BGK model. Since the flow has low Mach number, the statistical fluctuations dominates the DSMC solutions. Therefore, we have obtained 20 independent runs. In Figure 5.2 we have plotted the density, velocity and pressure obtained from the DSMC simulations and the BGK model using MLS and Hermite interpolations. We observe that the MLS interpolation scheme for the BGK model and DSMC results match perfectly, however, the Hermite interpolation gives some deviations from the solutions of the DSMC simulations.

5.3. Test 3. In this test case we have increased the density by factor 2 and 10 times compared to the Test cases 1 and 2 such that $\rho_l = 10^{-5}kg m^{-3}$ and $10^{-4}kg m^{-3}$, respectively. The corresponding Knudsen numbers are 0.01 and 0.001 on the left half of the domain and 8 times larger on the right half. For $\rho_l = 10^{-5}kg m^{-3}$ we have considered the 400 cells in the DSMC simulations and the same number of grids for the BGK model. Similarly, for $\rho_l = 10^{-4}kg m^{-3}$ we have considered the 1000 cells in the DSMC simulations and the 800 grids for the BGK model. The increase of the number of cells is due to the restriction that the DSMC cells must be smaller than the mean free path. Other parameters are same as in the earlier test cases.

For the DSMC simulations we have performed 20 independent runs. In Figures

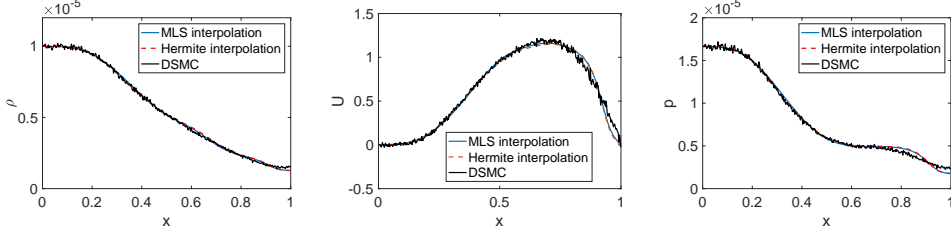


Fig. 5.3: Comparison of density, velocity and pressure obtained from MLS reconstruction, Hermite interpolation and DSMC for Knudsen number $Kn = 0.01$ on the left and $Kn = 0.08$ on the right.

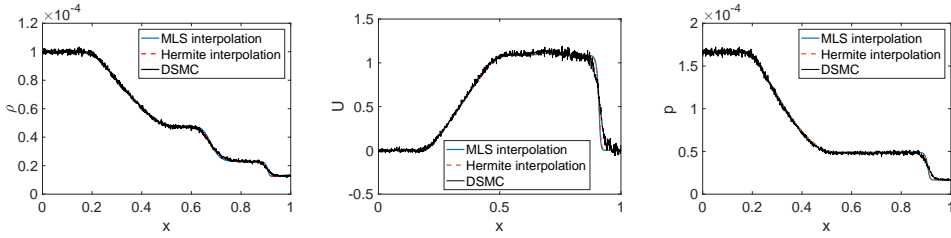


Fig. 5.4: Comparison of density, velocity and pressure obtained from MLS reconstruction, Hermite interpolation and DSMC for Knudsen number $Kn = 0.001$ on the left and $Kn = 0.008$ on the right.

5.3 and 5.4 we have plotted the numerical solutions from all three methods. We again observe that the DSMC solutions and the solutions of the BGK model obtained by MLS interpolation are closer than the Hermite interpolation.

5.4. Test 4. In this test case we consider $\rho_l = 1kg\ m^{-3}$ and $\rho_r = 0.125kg\ m^{-3}$. The corresponding left and right Knudsen numbers are 10^{-7} . and 8×10^{-7} , respectively. We note that the size of DSMC cells must be smaller than λ , so, we need at least 9×10^6 cells in this Knudsen numbers. The time step also has to be reduced accordingly. Moreover, the number of gas molecules is also very high and the computational time for the DSMC simulations becomes enormously high. . In one dimensional case, this is quite large number of cells. Therefore, we have not performed DSMC simulations in this case. However, there is no restriction of cell size for the semi Lagrangian scheme for the BGK model. We have again used 800 grids for the semi Lagrangian scheme for this smaller Knudsen numbers.

On the other hand for this small Knudsen numbers we can solve the continuum equations, for example, the compressible Euler equations. For the shock tube problem, the compressible Euler equations can be solved exactly. In Figure 5.5 we have again plotted the density, velocity and pressure at final time 0.17 seconds obtained from the MLS and Hermite interpolations together with the exact solutions of the compressible Euler equations. In the shock region all three solutions match perfectly, however, in the contact discontinuity and the rarefaction region, the MLS interpolation scheme gives better approximation than the Hermite interpolation scheme.

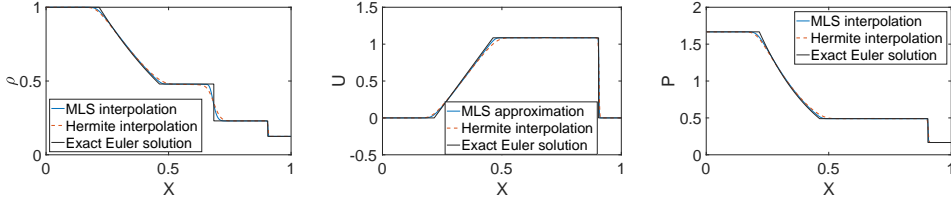


Fig. 5.5: Comparison of density, velocity and pressure obtained from MLS reconstruction, Hermite interpolation and the exact solutions of the compressible equations for Knudsen number $Kn = 10^{-7}$ on the left and $Kn = 8 \times 10^{-7}$ on the right.

5.5. Comparing solutions from continuous and discrete Maxwellian.

In all above examples we have considered the velocity grids $N_v = 20$ in all three directions the standard Maxwellian given by (2.2). Increasing the number of velocity grids do not help much in the accuracies of the solutions. However, smaller values of N_v affects the accuracies. This means we loose the conservative properties of the scheme. In this test case we have considered all parameters as in the Test 4. We have observed that $N_v = 20$ gives the solutions as close as the exact solutions of the compressible Euler equations. So, the solutions obtained from $N_v = 20$ are our reference solutions. We have decreased the values of N_v and compare the solutions with the reference solutions. The smallest one which gives the stable solutions is $N_v = 13$ for the case of the standard Maxwellian. But the solutions deviate from the reference solutions. For smaller values of N_v we loose the conservative properties. In other words, the moments obtained from the discrete summation in Eq. (3.7 - 3.11) are not exactly equal to the moments computed from the standard Maxwellian (2.2). To obtain conservative properties, one uses the discrete Maxwellian suggested by Mieussiens [12]. The discrete Maxwellian depends on five parameters, which are also related to the moments and the parameters are determined by solving the non-linear system of equations. Since the Jacobian matrix has very bad condition number, the standard Newton's method for solving non-linear system does not work, one has to use the back tracking line search algorithm [6].

In the case of three dimensional velocity space, the main drawback of the method is the memory problem as well as long computational time. Therefore, it is important to reduce the computational time as well as memory allocation. Thus we have considered the standard Maxwellian as well as discrete Maxwellian. If the number of velocity grid points is equal to 20 or above, we do not see much difference of the solutions obtained from the standard as well as the discrete Maxwellian. However, the discrete Maxwellian is requires more computational efforts than the standard Maxwellian because of the iterative method for solving nonlinear system of equations. If we choose the proper initial guess, the Newton iteration converges very fast. We observed that if we consider discrete Maxwellian with 13 velocity grids, the solutions are same as the ones obtained from the standard Maxwellian with 20 velocity grids. But with 13 velocity grids with standard Maxwellian, the solutions deviate from the reference solutions. In Figure 5.6 we have plotted the density, velocity and pressure obtained from the BGK model with discrete Maxwellian considering $N_v = 13$ and with the standard Maxwellian considering $N_v = 13$ together with the reference solutions. We see that the solutions obtained from the standard Maxwellian with $N_v = 13$ deviates from the reference solutions, while the solutions with the discrete Maxwellian with

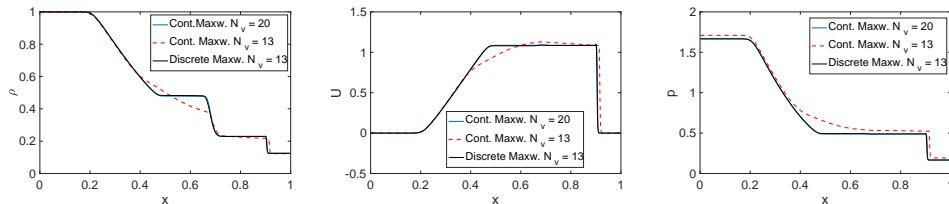


Fig. 5.6: Comparison of density, velocity and pressure from the BGK model considering continuous Maxwellian with $V_v = 20$ and $N_v = 17$ together with the solutions considering discrete Maxwellian with $N_v = 13$.

$N_v = 13$ are closer with the reference solutions (standard Maxwellian with $N_v = 20$). The computation is performed in *dualIntelXeonGold6132("Skylake")@2.6GHz* with intel fortran compiler. The total CPU to time with the standard Maxwellian having 20 velocity grids is 443 seconds while with the discrete Maxwellian with 13 velocity grids is 166 seconds. In higher dimensional cases the reduction of velocity grid points N_v is very important from the computation as well as memory allocation point of view.

6. Conclusion and Outlook . In this paper we have focussed on a meshfree method in the semi Lagrangian scheme for the BGK model for rarefied gas flows. The meshfree method is applied for the reconstruction steps as well as for the implementation of boundary conditions. The diffuse boundary conditions on the solid wall is applied. The meshfree approximation is based on the moving least squares (MLS) method. We have used a linear approximation. The advantage of the meshfree approximation is that we do not require regular distribution of grid points in the velocity space, which will be very important if the boundary moves in time or interface between gases and other medium changes in time. Another advantage of the meshfree method is that we do not need to add ghost points. We have presented also the linear piecewise Hermite interpolations in order to compare the results from the MLS interpolations. We observed that MLS gives better results than the Hermite interpolation. We have considered a problem in one dimensional physical space and three dimensional velocity space. Sod's shock tube problem is solved for several ranges of Knudsen numbers. No difference is found in the results obtained from regular and irregular grids in physical space. For larger Knudsen numbers the solutions of BGK model are compared with the solutions obtained from the DSMC method for the Boltzmann equation. The solutions obtained from MLS are closer to DSMC results than the Hermite interpolation. For a very small Knudsen number we have compared the solutions of BGK model with the exact solutions of the compressible Euler equations and the solutions have very good agreement. In this case also the MLS approximation gives better results than the Hermite interpolation. Moreover, we have studied the difference between the solutions obtained from the continuous and the discrete Maxwellian distribution. We found that the use of discrete Maxwellian allows us to reduce the number of grid points in velocity space without losing the accuracy in the solutions. The reduction of number of grid points is very important in higher dimensional physical spaces from the point of view of computational time and memory allocations.

Future works will be the extension of the method for higher order reconstruction

using WENO. Moreover, we are planning the extension of the method in higher dimensional physical spaces as well as the interaction of moving nano rigid particles immersed in a rarefied gas.

REFERENCES

- [1] H. Babovsky, *A convergence proof for Nanbus Boltzmann simulation scheme*, Eur. J. Mech., 8:41, 1989.
- [2] G. A. Bird, *Molecular Gas Dynamics and Direct Simulation of Gas Flows*, Oxford University Press, New York, 1994.
- [3] J. A. Carrillo, F. Vecil, *Non oscillatory interpolation methods applied to Vlasov-based models*, SIAM J. Sci. Comput., 27 (2005), 1071-1091.
- [4] C. Cercignani, R. Illner, M. Pulvirenti, *The Mathematical Theory of Dilute Gases*, Springer, 1994.
- [5] S. Chapman, T. W. Cowling, *The Mathematical Theory of Non-Uniform Gases*, Cambridge University Press, 1970.
- [6] J. E. Dennis, R. B. Schnabel, *Numerical Methods for Unconstrained Optimization and Non-linear Equations*, Prentice-Hall, 1983.
- [7] G. Dechriste', L. Mieussens, *Numerical simulation of micro flows with moving obstacles*, J. Phys.: Conf. Series 362 (2012) 012030.
- [8] S. M. Deshpande, V. Ramesh, K. Malagi, K. Arora, *Least squares kinetic upwind mesh-free method*, Defence Science Journal, Vol. 60, No. 6, pp. 583-597, 2010.
- [9] M. Gad-el Hak, *The fluid mechanics of microdevices-the freeman schola rlecture*, ASME J. Fluids Enggs., 121(403), 533, 1999.
- [10] E. P. Gross, P. L. Bhatnager, M.Krook, , Phys. Rev. 94, 511, 1954.
- [11] G. E. Karniadakis, A. Beskok, N. R. Aluru, *Microflows and Nanoflows, Fundamentals and Simulation*, Springer, New York, 2006.
- [12] L. Mieussens, *Discrete velocity model and implicit scheme for the BGK equation of rarefied gas dynamics*, Math. Models Methods Appl. Sci., 10 (2000), 1121-1149.
- [13] H. Neunzert, J. Struckmeier, *Particle methods for the Boltzmann equation*, Acta Numerica, page 417, 1995.
- [14] G. Russo, F. Filbet, *Semi-lagrangian schemes applied to moving boundary problems for the BGK model of rarefied gas dynamics*, Kinetic and Related Models, Amer. Inst. Math. Sci., Vol. 2, No. 1, pp 231-250, 2009.
- [15] G. A. Sod, *A survey of several finite difference methods for systems of nonlinear hyperbolic conservation laws*, J. Comp. Phys. 27 (1978), 1-31.
- [16] S. Tiwari, J. Kuhnert, *Modelling of two-phase flow with surface tension by Finite Point-set method (FPM)*. J. Comp. Appl. Math. 203 (2007), 376-386.
- [17] S. Tiwari, A. Klar, S. Hardt, *A particle-particle hybrid method for kinetic and continuum equations*, J. Comp. Phys. 228, (2009), 7109-7124.